CERTIFICATION OF ATTRIBUTION ROBUSTNESS FOR EUCLIDEAN DISTANCE AND COSINE SIMILARITY MEASURE

Anonymous authors
Paper under double-blind review

ABSTRACT

Model attribution is a critical component of deep neural networks (DNNs) for its interpretability to complex models. Recent works bring up attention to the security of attributions as they are vulnerable to attribution attacks that generate similar images with dramatically different attributions. Studies have been working on empirically improving the robustness of DNNs against those attacks. However, due to their lack of certification, the actual robustness of the model for a testing point is not known. In this work, we define *certified attribution robustness* for the first time that upper bounds the dissimilarity of attributions after the samples are perturbed by any noises within a certain region while the classification results remain the same. Based on the definition, we propose different approaches to certify the attributions using Euclidean distance and cosine similarity under both ℓ_2 and ℓ_∞-norm perturbations constraints. The bounds developed by our theoretical study are validated on three datasets (MNIST, Fashion-MNIST and CIFAR-10), and two different types of attacks (PGD attack and IFIA attribution attack). The experimental results show that the bounds certify the model effectively.

1 INTRODUCTION

Attribution methods play an important role in deep learning applications as one of the subareas of explainable AI. Practitioners use attribution methods to measure the relative importance among different features and to understand the impacts of features contributing to the model outputs. They have been widely used in a number of critical real-world applications, such as risk management (Bhatt et al., 2020), medical imaging (Sayres et al., 2019; Singh et al., 2020a) and drug discovery (Jiménez-Luna et al., 2020). In particular, attributions are supposed to be secure and resistant to external manipulation such that proper explanations can be applied to safety-sensitive applications. Regulations are also deployed in countries to enforce the interpretability of deep learning models for a 'right to explain' (Goodman & Flaxman, 2017). Although attribution methods have been extensively studied (Simonyan et al., 2014; Zeiler & Fergus, 2014; Lundberg & Lee, 2017; Shrikumar et al., 2017; Sundararajan et al., 2017; Zintgraf et al., 2017), recent works reveal that they are vulnerable to visually imperceptible perturbations that drastically alter the attributions and keep the model outputs unchanged (Ghorbani et al., 2019; Dombrowski et al., 2019).

Prior works (Chen et al., 2019; Boopathy et al., 2020; Ivankay et al., 2020; Singh et al., 2020b; Wang et al., 2020; Sarkar et al., 2021; Wang & Kong, 2022) investigate the attribution robustness based on empirical and statistical estimations over entire dataset. However, unlike certification in adversarial robustness (Zhang et al., 2018; Cohen et al., 2019; Singla & Feizi, 2020), current attribution robustness works are unable to guarantee the robustness of any arbitrary test point, perturbed or unperturbed. In this paper, we study the problem of certified attribution robustness. Specifically, given a trained model and an image sample, we propose theoretical upper bounds of the attribution deviations from the unperturbed ones. As far as we know, this is the first attempt to provide a guarantee of attribution robustness.

In this paper, we first formulate the problem of certified attribution robustness. We characterize the certified attribution robustness as an upper bound for the changes of attributions after the samples are perturbed. We analyze two cases including with and without label constraint, which refers to

the classification labels being unchanged and changed, respectively, after the original samples are attacked. For each case, two mostly used perturbation constraints, ℓ_2 and ℓ_∞-norm, are considered to compute the upper bound. For ℓ_2-norm constraint, our approach is based on the first-order Taylor series of model attribution, and a tight upper bound ignoring the label constraint is computed from the singular value of the attribution gradient. ℓ_∞-norm constraint is more complicated because the upper bound is a solution of a concave quadratic programming with box constraints, which is an NP-hard problem. Thus, two relaxation approaches are proposed. Moreover, a more restricted certification constrained on the unchanged label is studied. In this study, Euclidean distance and cosine distance, which are also employed in the previous empirical studies (Chen et al., 2019; Singh et al., 2020b; Wang & Kong, 2022), are used as dissimilarity functions to measure attribution difference for certification. We summarize the contributions of this paper as follows:

- We formally define the certifiable attribution robustness problem as an upper bound of attributional differences. According to the best knowledge of the authors, it has not been studied before.
- The tight upper bounds for ℓ_2-norm constrained attacks with and without classification label constraints are proposed based on the first-order Taylor series. The proposed bound generalizes to all gradient-based attribution methods.
- Two different approaches are provided to bound the ℓ_∞-norm constrained attacks above, which uses an ℓ_p-norm relaxation and a mathematical property of the quadratic form.
- The experimental results show that the upper bounds derived in this paper can effectively certify the tested samples and models.

The rest of this paper is organized as follows. We start with an introduction to notations and related works. The formulation of certified attribution robustness is defined in Sec. 3. Specific certification methods in different scenarios are provided in Sec. 4. In Sec. 5, detailed experimental results are presented and the paper concludes in Sec. 6.

2 Preliminaries and Related Works

We consider a twice-differentiable classifier f that maps the input set $\mathcal{D} = \left\{(\boldsymbol{x}^{(i)}, y^{(i)})\right\}_{i=1}^{n}$ to the logits, $f : \mathbb{R}^d \to \mathbb{R}^k$, where $\boldsymbol{x}^{(i)} \in \mathbb{R}^d$ and $y^{(i)} \in \{1, \ldots, k\}$ represent the i-th sample and its ground truth label. The non-bold version x_k represents the k-th feature of $\boldsymbol{x}$ and f_y is the logit at label y. The model attribution of the input sample given label y is computed by $g^y : \mathbb{R}^d \to \mathbb{R}^d$, and we denote the attribution of $\boldsymbol{x}$ by $g^y(\boldsymbol{x})$.

2.1 Model Attribution

The model attribution studies the importance of each input feature x_i that contributes to the final output $f_y(\boldsymbol{x})$. We can classify the most used attribution methods into two categories, perturbations-based methods (Zeiler & Fergus, 2014; Zintgraf et al., 2017) and backpropagation-based methods (Shrikumar et al., 2017; Bach et al., 2015), which include gradient-based methods. In particular, in this paper, we focus on the most commonly used gradient-based attribution methods, saliency map (SM), gradient*input and integrated gradient (IG). Saliency map (Simonyan et al., 2014) is defined as the gradients of output with respect to the input. Gradient*input (Shrikumar et al., 2016) is computed by element-wise multiplication of input features and the gradients. Integrated gradients (Sundararajan et al., 2017) is defined as line integral of gradients from a baseline image $\boldsymbol{a}$ to the input image $\boldsymbol{x}$ weighted by their difference[1]. It is worth noting that IG satisfies the axiom of completeness, $\sum_i g_i^y(\boldsymbol{x}) = f_y(\boldsymbol{x})$, which builds a direct connection between the attributions and model outputs. The mathematical expressions and examples of the attribution methods are given in Table 1.

2.2 Attribution robustness

It has been discovered in the literature that model attributions can be easily sabotaged by adversaries. Similar to adversarial examples (Goodfellow et al., 2015), human-indistinguishable perturbations

[1]The baseline is chosen to be a black image ($\boldsymbol{a} = \boldsymbol{0}$) in this paper if not specifically stated. Without loss of generality, $f_y(\boldsymbol{a}) = 0$.

Table 1: Mathematical expressions and visual examples of the selected attribution methods. Attributions have been taken absolute values and are presented heatmaps to reflect relative importance among pixels. The baseline $\boldsymbol{a}$ of IG is chosen as a black image. $\otimes$ denotes the element-wise multiplication.

Original image	Saliency map $\nabla f_y(\boldsymbol{x})$	Input*gradient $\boldsymbol{x} \otimes \nabla f_y(\boldsymbol{x})$	Integrated gradients $(\boldsymbol{x}-\boldsymbol{a}) \otimes \int_0^1 \nabla f_y(\boldsymbol{a}+\alpha(\boldsymbol{x}-\boldsymbol{a}))\, d\alpha$
	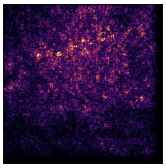	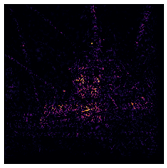	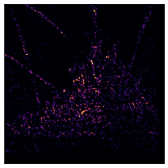

can be also augmented to natural images that, though classification results remain unchanged, misdirect the model attributions towards meaningless interpretations (Ghorbani et al., 2019) or any predefined arbitrary patterns which are unrelated to the original images (Dombrowski et al., 2019).

To mitigate the threat of being attacked, researchers have also worked on training attribution robust models. The most considered techniques are adapted from adversarial training (Madry et al., 2018), and they minimize the differences between original and the worst-case perturbed attributions. Chen et al. (2019) and Boopathy et al. (2020) consider the ℓ_1-norm distance to measure the difference between attributions, and Ivankay et al. (2020) uses Pearson correlation coefficient. Singh et al. (2020b) and Wang et al. (2020) choose ℓ_2-norm distance, where the former upper bounds the difference using a spatial correlation between image and attribution, and the latter shows the smoothness of the decision surface is related to attribution robustness based on a geometric understanding. Wang & Kong (2022) emphasizes the directions of attributions using the relationship between Kendall's rank correlation and cosine similarity and protects the attribution based on the latter. However, none of the aforementioned methods defines a certification of attribution robustness. More clearly, the attributions are not guaranteed to be protected for all perturbations within the allowable region that do not alter the classification outputs.

3 Formulation of Certifiable Attribution Robustness

In this section, we introduce the problem of certifying attribution robustness. Recall that adversaries incapacitate the attributions of neural networks by adding imperceptible noises to natural images. For an attributional robust model, on the contrary, the imperceptible noises should not change the interpretability of attributions, *i.e.*, images perturbed by noises should provide *similar* attributions as the original ones. To certify such resistance against adversaries, it is essential to find an upper bound that represents the worst-case dissimilarity of attributions after the original images being perturbed. Thus, we define the certifiable attribution robustness as follows.

Definition 1 (Certified attribution robustness)**.** Given a trained neural network f, a fixed allowable region for perturbation $\boldsymbol{\delta}$, $\mathcal{B}_\varepsilon = \{\boldsymbol{\delta} : \|\boldsymbol{\delta}\|_p \leq \varepsilon\}$, and an input sample $\boldsymbol{x}$, the *certified attribution robustness* is defined to be an upper bound $T(\varepsilon; \boldsymbol{x})$ that, for all perturbations $\boldsymbol{\delta} \in \mathcal{B}_\varepsilon$, if $\arg\max_k f_k(\boldsymbol{x}) = \arg\max_k f_k(\boldsymbol{x}+\boldsymbol{\delta})$, then their corresponding attributions satisfy that $D(g^y(\boldsymbol{x}), g^y(\boldsymbol{x}+\boldsymbol{\delta})) \leq T(\varepsilon; \boldsymbol{x})$.

In the above definition, $D(\cdot,\cdot)$ is a dissimilarity metric that measures the difference between two attributions, where a smaller value indicates that two attributions are more similar and represent closer meaningful interpretations. T is a function with respect to the threshold ε and $\boldsymbol{x}$. The definition formalizes the guarantee of attribution robustness, where when the model is more robust, the model attributions being attacked are less likely to be misled. More precisely, when being attacked, the change of attribution is certified to be bounded above and the smaller upper bound indicates the more attributional robust model.

Based on the above definition, the certified attribution robustness $T(\varepsilon; \boldsymbol{x})$ can be found by solving the optimization problem

$$\begin{aligned} \max_{\boldsymbol{\delta}} \quad & D(g^y(\boldsymbol{x}), g^y(\boldsymbol{x}+\boldsymbol{\delta})) \\ \text{s.t.} \quad & \|\boldsymbol{\delta}\|_p \leq \varepsilon \\ & \arg\max_k f_k(\boldsymbol{x}) = \arg\max_k f_k(\boldsymbol{x}+\boldsymbol{\delta}) \end{aligned} \tag{1}$$

We refer the first constraint $\|\boldsymbol{\delta}\|_p \leq \varepsilon$ to the norm constraint and the second one to the label constraint as it requires the unchanged label after being perturbed. An alternative formulation of this problem is to find the maximum ε subject to $D(g^y(\boldsymbol{x}), g^y(\boldsymbol{x}+\boldsymbol{\delta})) \leq \omega$ where ω is a predefined threshold. In following sections, we attempt to solve the optimization problem (1) using the two mostly used norm constraints on the perturbations, ℓ_2 and ℓ_p, *i.e.*, $\|\boldsymbol{\delta}\|_2 \leq \varepsilon$ and $\|\boldsymbol{\delta}\|_\infty \leq \varepsilon$. For the dissimilarity metric, we choose from previously used attribution measurements, the Euclidean distance and the cosine distance. The results can be converted directly to the alternative formulation, and we defer the procedures to Appendix E.

4 Certifiable Attribution Robustness

4.1 ℓ_2-Norm Certification without the Label Constraint

To start with, the certification without label constraints is studied. This will provide a looser bound since, intuitively, stronger adversaries are allowed to perturb the samples that may change the classification results. While perturbations are only restricted in a small region where the perturbed samples are still indistinguishable to humans, attributions are more vulnerable and could still be malicious. The upper bound for ℓ_2-norm constrained case is a straightforward derivation of the first-order Taylor series of attribution functions. The following theorem provides a tight bound for attribution robustness assuming that the attribution function is locally linear.

Theorem 1. *Given a twice-differentiable classifier $f : \mathbb{R}^d \to \mathbb{R}^k$, and its attribution g^y on label y, assume that g^y is locally linear within the neighborhood of $\boldsymbol{x}$, $\mathcal{B}_\varepsilon(\boldsymbol{x}) = \{\boldsymbol{x}+\boldsymbol{\delta} | \|\boldsymbol{\delta}\|_2 \leq \varepsilon\}$, then for all perturbations $\|\boldsymbol{\delta}\|_2 \leq \varepsilon$,*

$$\|g^y(\boldsymbol{x}+\boldsymbol{\delta}) - g^y(\boldsymbol{x})\|_2 \leq \xi_{max}\varepsilon,$$

where ξ_{max} is the largest singular value of $H = \nabla g^y(\boldsymbol{x})$.

Proof. Based on the Taylor series of $g^y(\boldsymbol{x})$ and the above condition, we have

$$\|g^y(\boldsymbol{x}+\boldsymbol{\delta}) - g^y(\boldsymbol{x})\|_2^2 \leq \|\boldsymbol{\delta}^\top \nabla g^y(\boldsymbol{x})\|_2^2 = \boldsymbol{\delta}^\top \nabla g^y(\boldsymbol{x}) \nabla g^y(\boldsymbol{x})^\top \boldsymbol{\delta} \tag{2}$$

$$= \frac{\boldsymbol{\delta}^\top}{\|\boldsymbol{\delta}\|_2} P \frac{\boldsymbol{\delta}}{\|\boldsymbol{\delta}\|_2} \cdot \|\boldsymbol{\delta}\|_2^2 \tag{3}$$

$$\leq \lambda_{max}\|\boldsymbol{\delta}\|_2^2 \leq \lambda_{max}\varepsilon^2 \tag{4}$$

where λ_{max} is the largest eigenvalue of $P = HH^\top = \nabla g^y(\boldsymbol{x}) \nabla g^y(\boldsymbol{x})^\top$, and $\boldsymbol{v}_{max}$ is the corresponding eigenvector. The equality in Eq. 4 is achieved when $\boldsymbol{\delta}$ is $\varepsilon \boldsymbol{v}_{max}$ or $-\varepsilon \boldsymbol{v}_{max}$. Since the singular values of H are equal to the square root of the eigenvalues of P, then,

$$\|g^y(\boldsymbol{x}+\boldsymbol{\delta}) - g^y(\boldsymbol{x})\|_2 \leq \sqrt{\lambda_{max}}\varepsilon = \xi_{max}\varepsilon. \tag{5}$$

□

Note that the local linearity of attribution function is a weak assumption for both attribution and adversarial robust models since most of the defense methods (Qin et al., 2019; Wang et al., 2020) attempt to smoothen the functions. In addition, when the magnitude of perturbation $\boldsymbol{\delta}$ is constrained to small size, the magnitude of the higher-order Taylor remainders is negligible. We include the empirical results evaluating this assumption in Appendix B. Furthermore, we also provide a generalization of the theorem that bounds the attribution differences as a function of a constant $c \geq 1$ that measures the error margin of the first-order Taylor series in Appendix B.2, which can be applied similarly on all other results in this work.

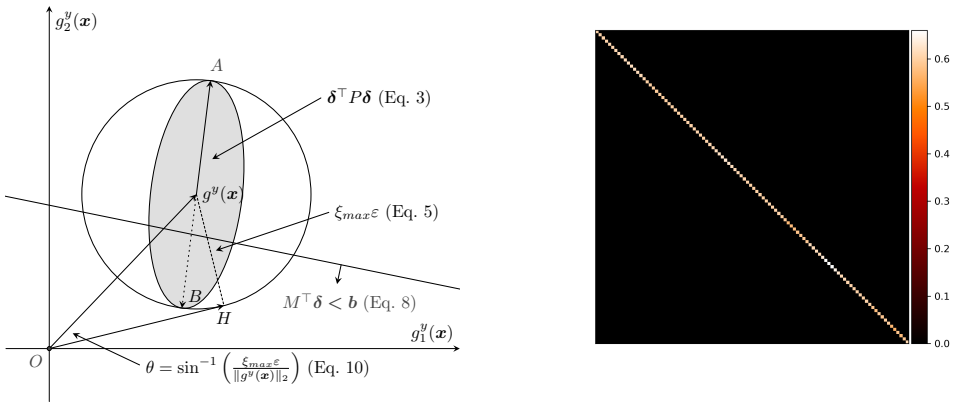

(a) (b)

Figure 1: (a) 2D illustration of certification on Euclidean distance and cosine distance. (b) Visualization of the absolute values of gradient IG as a heat map. The gradient is generated using CIFAR-10 (3072×3072), and the values are normalized to $[0, 1]$. Here the first 100 dimensions of each axis are plotted for better visualization, and more figures and mathematical analysis are in Appendix C.

We also notice that the above theorem uses the gradient of attribution $H = \nabla g^y(\boldsymbol{x})$, which is also the Hessian matrix $\nabla^2 f_y(\boldsymbol{x})$ when the attribution is chosen as saliency maps and can be computed easily for other gradient-based attribution methods. Moreover, the second-order derivatives can be zeros for ReLU networks. In this work, the non-linearity functions are replaced by softplus function $f(\boldsymbol{x}; \beta) = \frac{1}{\beta}\log(1 + e^{\beta \boldsymbol{x}})$ as in Dombrowski et al. (2019). A 2D example of the upper bound is illustrated in Fig. 1a. The optimum solution is in the same direction as the semi-major axis of the ellipse, which represents $\boldsymbol{\delta}^\top P\boldsymbol{\delta}$. The circle represents the 2D Euclidean ball bounded by $T(\varepsilon; \boldsymbol{x})$, which is derived from the length of the semi-major axis.

4.2 ℓ_∞-Norm Certification without the Label Constraint

The upper bound for ℓ_∞ constrained case is more complicated as $\|\boldsymbol{\delta}\|_\infty \leq \varepsilon$ defines a box constraints inequality system that $-\varepsilon \leq \delta_i \leq \varepsilon$ for all i. If we still consider the quadratic form derived from the first-order Taylor series as in Sec. 4.1, the above optimization problem (1) turns into a concave quadratic programming with box constraints, which is NP-hard (Pardalos & Vavasis, 1991). In order to compute the upper bound efficiently, we consider a loose relaxation of p-norms.

Corollary 1. *Given a twice-differentiable classifier $f : \mathbb{R}^d \to \mathbb{R}^k$, and its attribution g^y on label y, assume that g^y is locally linear within the neighborhood of $\boldsymbol{x}$, $\mathcal{B}_\varepsilon(\boldsymbol{x}) = \{\boldsymbol{x} + \boldsymbol{\delta} | \|\boldsymbol{\delta}\|_p \leq \varepsilon\}$, then for all perturbations $\|\boldsymbol{\delta}\|_p \leq \varepsilon$ that $p > 2$, $\|g^y(\boldsymbol{x} + \boldsymbol{\delta}) - g^y(\boldsymbol{x})\|_2 \leq d^{\frac{1}{2}-\frac{1}{p}}\xi_{max}\varepsilon$, where ξ_{max} is the largest singular value of $H = \nabla g^y(\boldsymbol{x})$.*

The proof of the relaxation of p-norm and Corollary 1 can be found in Appendix A.1. Note that this corollary not only avoids the NP-hard problem for ℓ_∞-norm constraint, but it is also a general upper bound for p-norm constraint on $\boldsymbol{\delta}$ when $p > 2$. However, it is also noticed that the upper bound increases with respect to the input sample dimension. The multiplication factor for ℓ_∞ is $\sqrt{d}$. For high-dimensional input samples, the provided method would scale up to an extremely loose upper bound that can be trivial but meaningless for the robust certification. To better certify the attribution in the ℓ_∞-norm case, we provide a tighter upper bound using the sparsity of attribution gradients.

Theorem 2. *Given a twice-differentiable classifier f, its attribution on label y, g^y, and the gradient $H = \nabla g^y$, assume that g^y is locally linear within the neighborhood of $\boldsymbol{x}$, $\mathcal{B}_\varepsilon(\boldsymbol{x}) = \{\boldsymbol{x} + \boldsymbol{\delta} | \|\boldsymbol{\delta}\|_\infty \leq \varepsilon\}$, then for all perturbations $\|\boldsymbol{\delta}\|_\infty \leq \varepsilon$,*

$$\|g^y(\boldsymbol{x} + \boldsymbol{\delta}) - g^y(\boldsymbol{x})\|_2 \leq \varepsilon \sqrt{\sum_{i,j} |P_{ij}|}. \tag{6}$$

where $P = HH^\top$ and the equality is taken at $\boldsymbol{\delta} = (\pm\varepsilon, \ldots, \pm\varepsilon)^\top$.

The proof is deferred to Appendix A.2. This upper bound as the summation of absolute values of the matrix $P = \nabla g^y(\boldsymbol{x}) \nabla g^y(\boldsymbol{x})^\top$ is shown to be tighter than that given in Corollary 1 since P is a diagonal-dominated and positive semi-definite matrix (see Fig. 1b), which implies that $|P_{ii}| \approx \lambda_i$.

4.3 Certification with the Label Constraint

In this section, we generalize our certification to the case that labels are not changed after the samples are perturbed. Here, only attribution methods satisfying the axiom of completeness are studied as the axiom provides a direct connection between attributions and model outputs, *i.e.*, $\sum_i g_i^y(\boldsymbol{x}) = f_y(\boldsymbol{x})$. The following proposition gives a sufficient condition to ensure that the classification result remains unchanged after the sample is perturbed.

Proposition 1. *Denote the gradient-based attribution satisfying the completeness axiom of $\boldsymbol{x}$ on ground truth label y by $g^y(\boldsymbol{x})$, and the attribution on a different label y' by $g^{y'}(\boldsymbol{x})$. Given the perturbation $\boldsymbol{\delta}$, assume that g^y is locally linear within the neighborhood of $\boldsymbol{x}$, $\mathcal{B}_\varepsilon(\boldsymbol{x}) = \{\boldsymbol{x} + \boldsymbol{\delta} | \|\boldsymbol{\delta}\|_p \leq \varepsilon\}$, the classification result of $\boldsymbol{x} + \boldsymbol{\delta}$ does not change from y to y' if*

$$\left(\left(\nabla g^{y'}(\boldsymbol{x}) - \nabla g^y(\boldsymbol{x}) \right) \Delta \right)^\top \boldsymbol{\delta} < f_y(\boldsymbol{x}) - f_{y'}(\boldsymbol{x}), \tag{7}$$

where Δ is an all one vector, $\Delta = (1, \ldots, 1)^\top \in \mathbb{R}^d$.

The full proof can be found in Appendix A.3. Note that the inequality is linear to $\boldsymbol{\delta}$ and we denote $M = (\nabla g^{y'}(\boldsymbol{x}) - \nabla g^y(\boldsymbol{x}))\Delta$ and $b = f_y(\boldsymbol{x}) - f_{y'}(\boldsymbol{x})$ for simplicity, *i.e.*, $M^\top \boldsymbol{\delta} < b$. To certify the attribution differences after the sample is perturbed by noise $\boldsymbol{\delta}$ in ℓ_2-norm ball, *i.e.*, $\|\boldsymbol{\delta}\|_2 \leq \varepsilon$, the upper bound can be formulated by rewriting the optimization problem (1) as the optimal value of the following quadratic programing with concave objective function and a system of linear constraints for all labels different from y,

$$\max_{\boldsymbol{\delta}} \ \boldsymbol{\delta}^\top P \boldsymbol{\delta} \quad \text{s.t. } \|\boldsymbol{\delta}\|_2 \leq \varepsilon \text{ and } M^\top \boldsymbol{\delta} < b. \tag{8}$$

To simplify the computation, in this work, we only consider the second best label y', *i.e.*, $y' = \arg\max_{k \in \{1,\ldots,c\} \setminus y} f_k(\boldsymbol{x})$. In such case, the constraint $M^\top \boldsymbol{\delta} < b$ defines a half-space. Recall that Theorem 1 states that the upper bound in ℓ_2-norm certification without label constraint is $\xi_{max}\varepsilon$, and we noticed that this bound is achieved at two opposite vectors $\boldsymbol{\delta}^* = \varepsilon \boldsymbol{v}_{max}$ or $\boldsymbol{\delta}^* = -\varepsilon \boldsymbol{v}_{max}$. Thus, at least one of these two vectors lies in the half-space defined by the linear constraint (see point A and B in Fig. 1a. Therefore, the upper bound provided in Theorem 1 is also achieved even if the label constraint is added, *i.e.*, the optimal value of optimization problem (8) is also $\xi_{max}\varepsilon$.

The certification of ℓ_p-norm constrained case can be derived similarly. The less tight upper bound is still achievable at $d^{\frac{1}{2}-\frac{1}{p}}\xi_{max}\varepsilon$ as in Corollary 1. Generalizing the ℓ_∞-norm constrained upper bound using Eq. 6 is simpler. According to Theorem 2, there are 2^d different optimal solutions that achieve the optimum and they are the corners of the ℓ_∞-norm box. As long as the feasible region is non-empty, there exists at least one corner of the box lying inside the feasible region, and the optimum value is achieved. Similarly, given a d-dimensional ℓ_∞-norm box, and k label constraints that each separates the entire space into two half-spaces, if at least one corner of the box lies within the feasible region, the optimum value is attainable.

4.4 Certification Based on Cosine Distance

In the previous parts of this section, we discussed several cases in certified attribution robustness based on Euclidean distance. It is mentioned in Wang & Kong (2022) that cosine similarity (D_s) is a better metric to measure the difference of attributions as it emphasizes the relative importance among different features rather than the absolute magnitude of each individual feature. Our method can be trivially extended to the scenarios using cosine distance ($D_c = 1 - D_s(g^y(\boldsymbol{x} + \boldsymbol{\delta}), g^y(\boldsymbol{x}))$) as the dissimilarity function D defined in the formulation (1) with simple modifications.

Corollary 2. *Given a twice-differentiable classifier $f : \mathbb{R}^d \to \mathbb{R}^k$ and its attribution g^y on label y, for all perturbations $\|\boldsymbol{\delta}\|_p \leq \varepsilon$, if the Euclidean distance of $g^y(\boldsymbol{x} + \boldsymbol{\delta})$ and $g^y(\boldsymbol{x})$ is upper bounded by $T(\varepsilon; \boldsymbol{x})$, and $0 \leq T(\varepsilon; \boldsymbol{x}) \leq \|g^y(\boldsymbol{x})\|_2$, then their cosine distance (D_c) is upper bounded by*

$$D_c(g^y(\boldsymbol{x} + \boldsymbol{\delta}), g^y(\boldsymbol{x})) \leq 1 - \sqrt{1 - \frac{T(\varepsilon; \boldsymbol{x})^2}{\|g^y(\boldsymbol{x})\|_2^2}}. \tag{9}$$

Table 2: Evaluation of certification without the label constraint.

	SM					Input*gradient					IG				
	$\widehat{T}_e$	T_e	T'_e	$\widehat{T}_c$	T_c	$\widehat{T}_e$	T_e	T'_e	$\widehat{T}_c$	T_c	$\widehat{T}_e$	T_e	T'_e	$\widehat{T}_c$	T_c
ℓ_2	0.09	0.31	0.34	6.88	7.41	0.07	0.46	0.46	0.51	2.60	0.02	0.17	0.17	1.80	3.84
ℓ_∞	0.41	0.85	-	21.87	27.09	0.07	0.69	-	7.03	50.59	0.25	0.52	-	23.24	35.00

This upper bound is valid when the assumption that $0 \leq T(\varepsilon; \boldsymbol{x}) \leq \|g^y(\boldsymbol{x})\|_2$ is satisfied, *i.e.*, the variation of attribution distance is smaller than the original attribution. As shown in Fig. 1a, the angle between original and perturbed attributions is bounded by θ computed from the corollary.

5 Experimental Results

In this section, we evaluate the effectiveness of our certification by numerical experiments under both ℓ_2 and ℓ_∞-norms. Same as in the previous sections, we evaluate the certification under the local linearity assumption, which omits the higher-order remainder of Taylor series. In the following results, we compute the theoretical upper bound for adversarial robust models and attributional robust models, including *Adversarial Training* (AT) (Madry et al., 2018), IG-NORM (Chen et al., 2019), *Adversarial Attributional Training* with robust training loss (AdvAAT) (Ivankay et al., 2020), *Attributional Robustness Training* (ART) (Singh et al., 2020b), TRADES (Zhang et al., 2019) and *Integrated Gradients Regularizer* (IGR) (Wang & Kong, 2022). We follow previous attribution robustness studies to use ResNet-18 to evaluate CIFAR-10 (Krizhevsky, 2009), and use the neural network with four convolutional layers followed by three fully-connected layers to evaluate MNIST (LeCun et al., 2010) and Fashion-MNIST (Xiao et al., 2017).

For each selected model, the theoretical upper bounds for both Euclidean distance and cosine distance are computed. We convert the cosine values to degrees for easier comparison. The theoretical bounds are compared with corresponding sample distances to verify the effectiveness of the bounds. We denote the theoretical upper bounds for Euclidean distance and cosine distance as T_e and T_c, respectively. The ℓ_2 PGD-20 attack (Madry et al., 2018) is implemented for ℓ_2-norm bounded certification. The 200-step IFIA with the top-k intersection as dissimilarity function (Ghorbani et al., 2019) is implemented for ℓ_∞-norm bounded certification, where k is 100 for MNIST and Fashion-MNIST and 1000 for CIFAR-10. Each sample is attacked 20 times and the mean distance is computed. The sample mean distances of the entire dataset under corresponding attacks are denoted by $\widehat{T}_e$ and $\widehat{T}_c$, respectively. All the experiments are implemented on NVIDIA GeForce RTX 3090 (Source code will be provided later).

In addition, we also provide a generalization of the proposed bounds based on the generalization of Theorem 1 (Appendix B.2) that adaptively multiply a scalar c for an given input $\boldsymbol{x}$ in case that the weak assumption is violated in rare cases. Explicitly, the adaptive value of c for i-th sample is given as follows (details in Appendix B.3)

$$c^{(i)} = \max\left\{1, \frac{\|g^y(\boldsymbol{x}^{(i)} + \varepsilon \boldsymbol{v}^{(i)}_{max}) - g^y(\boldsymbol{x}^{(i)})\|_2}{\xi^{(i)}_{max}\varepsilon}\right\}. \tag{10}$$

5.1 Evaluation of Certification without the Label Constraint

We first evaluate the certification without label constraints, which can be applied to any gradient-based attribution method. Here three methods are evaluated, saliency map, input*gradient and integrated gradients. We provide the certification of TRADES+IGR on CIFAR-10 to validate the bounds as in Table 2, and leave the other models in Appendix D.1. We use the unlabelled certification introduced in Theorem 1 and 2 to compute $T_e = \xi_{max}\varepsilon$ and extend it to T_c using Eq. 9. The perturbation size is chosen to be 0.1 for ℓ_2 and 0.25 for ℓ_∞. The generalized upper bound $T'_e = c\xi_{max}\varepsilon$ (Eq. 10) is also provided for ℓ_2 case, and is not necessary for ℓ_∞ case. As we observe in the table, the proposed certification is valid for different attribution methods and both Euclidean and cosine distances are well-bounded. More precisely, none of the ℓ_∞ perturbed attributions is outside theoretical bound and none of the ℓ_2 perturbed attributions is outside the generalized bound.

Table 3: Evaluation of ℓ_2-norm certification with the label constraint. The numbers in the brackets indicate the percentages that attacked attribution is outside the T_e.

Model	$\widehat{T}_e$	T_e	T'_e	$\widehat{T}_c$(deg)	T_c(deg)
$\varepsilon = 0.05$		MNIST			
AT	0.0685	0.1537 [2.25%]	0.1596	3.6935	7.0951
IG-NORM	0.1158	0.2888 [2.00%]	0.2967	3.3174	7.2615
ART	0.0626	0.3591 [6.00%]	0.3702	2.3923	6.8657
AdvAAT	0.0876	0.3269 [6.20%]	0.3404	1.9034	6.8992
TRADES	0.1620	0.5060 [1.68%]	0.5271	2.8374	6.9988
TRADES+IGR	0.1784	0.4964 [1.32%]	0.5145	2.9075	6.9779
$\varepsilon = 0.05$		Fashion-MNIST			
AT	0.0659	0.0700 [2.19%]	0.0869	10.1442	12.9577
IG-NORM	0.1181	0.1789 [0.00%]	0.1789	6.6002	8.8043
AdvAAT	0.1115	0.1735 [6.20%]	0.1858	5.8544	9.3692
ART	0.0940	0.1387 [0.94%]	0.1411	5.4507	9.8234
TRADES	0.0626	0.0963 [4.16%]	0.1184	8.3521	12.0991
TRADES+IGR	0.0403	0.0453 [1.91%]	0.0507	7.7302	8.8411
$\varepsilon = 0.1$		CIFAR-10			
AT	0.0392	0.2532 [0.09%]	0.2533	2.7335	4.7724
IG-NORM	0.0149	0.1582 [0.42%]	0.1621	1.6505	4.3711
AdvAAT	0.0374	0.2386 [0.06%]	0.2386	0.2847	3.8202
ART	0.0733	0.2278 [0.00%]	0.2278	0.5918	4.2123
TRADES	0.0264	0.1734 [0.16%]	0.1734	1.9084	3.8686
TRADES+IGR	0.0240	0.1692 [0.09%]	0.1692	1.8011	3.8384

5.2 Evaluation of ℓ_2-Norm Bounded Certification with the Label Constraint

To certify the attributions of samples being attacked by ℓ_2-norm constrained perturbations, we use the method provided in Sec. 4.3 and 4.4 to obtain the theoretical upper bounds for both Euclidean distance ($T_e = \xi_{max}\varepsilon$) and cosine distance ($T_c$ in Eq. 9). Integrated gradients (IG) is chosen here as the certification with the label constraint is based on the axiom of completeness. Besides, as discussed in Sec. 4.1, the percentages of attacked attribution outside T_e are provided, and the generalized bound is also calculated and denoted by $T'_e = c\xi_{max}\varepsilon$. Since T'_e bounds all the attacked attributions, *i.e.*, 100% for all the models, we do not report the percentages in the table. From Table 3, we observe the following results. (i) The percentages are low, which supports our assumption in Sec. 4.1 that g^y is locally linear. (ii) The computed upper bounds for both Euclidean (T'_e) and cosine distance (T_c) successfully certify the attribution differences for every dataset and every model. In addition, we also show the minimum Euclidean gaps between samples and bounds in Appendix D.3 to illustrate that the tightness of the proposed bounds.

5.3 Evaluation of ℓ_∞-Norm Bounded Certification with the Label Constraint

We certify the attributions of samples under ℓ_∞ attacks in this subsection. Instead of the much looser bound derived from ℓ_p-norm relaxation (Corollary 1), the upper bound is computed from $T_e = \varepsilon\sqrt{\sum |P_{ij}|}$ as introduced in Sec. 4.3 and 4.4 . Moreover, the empirical attribution robustness is also provided using Kendall's rank correlation (Kendall, 1948) for comparison of theoretical and empirical protection. It should be emphasized that all the previous attribution robustness studies are based on ℓ_∞-norm constraints. Kendall's rank correlation is used to measure the difference between the original attributions and the attributions attacked by IFIA under ℓ_∞ constraints. From the results in Table 4, we see that the computed theoretical upper bounds are valid certifications of the attributions. For each dataset and each model, the sample mean of attribution distances is strictly smaller than the theoretical distance. Because of the relaxation, all attacked attributions are bounded by T_e. There is no outlier, and there is no need to use the generalized bound T'_e. Moreover, the

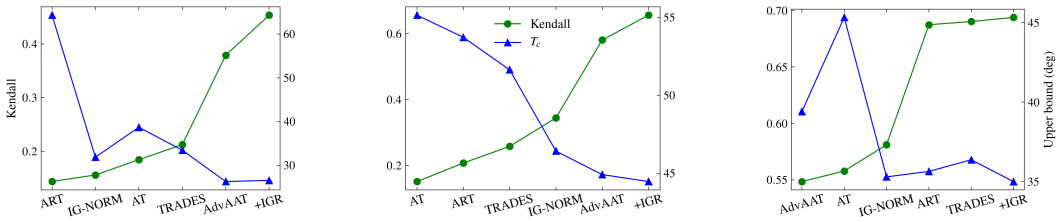

(a) MNIST (b) Fashion-MNIST (c) CIFAR-10

Figure 2: Comparison between Kendall's rank correlation and the theoretical bound of cosine distance. For clear comparison, we convert the cosine distance to angles in degrees.

Table 4: Evaluation of ℓ_∞-norm certification with the label constraint.

Model	Kendall	$\widehat{T}_e$	T_e	$\widehat{T}_c$(deg)	T_c(deg)
$\varepsilon = 0.05$			MNIST		
AT	0.1846	0.3461	0.7752	15.3616	38.7024
IG-NORM	0.1562	0.6836	1.2046	16.4506	31.8791
AdvAAT	0.3791	1.6269	2.1992	11.3173	26.3000
ART	0.1439	1.4193	2.8218	12.8025	64.3115
TRADES	0.2127	1.1779	2.2216	15.9881	33.4681
TRADES+IGR	0.4537	1.2991	2.0386	17.5923	26.5748
$\varepsilon = 0.05$			Fashion-MNIST		
AT	0.1516	0.0990	0.2802	18.9720	55.1501
IG-NORM	0.3446	0.2384	0.8819	12.6023	46.4270
AdvAAT	0.5810	0.1938	0.9206	9.4499	44.9184
ART	0.2079	0.1660	0.7215	9.6582	53.7281
TRADES	0.2582	0.1042	0.4536	13.7010	51.6448
TRADES+IGR	0.6565	0.0722	0.2526	15.0947	44.4703
$\varepsilon = 0.1$			CIFAR-10		
AT	0.5578	0.4058	0.7649	26.6195	45.3223
IG-NORM	0.5811	0.1997	0.4783	21.6311	35.2981
AdvAAT	0.5484	0.2293	0.5211	28.7342	39.3981
ART	0.6875	0.3128	0.6734	31.0090	35.6422
TRADES	0.6903	0.2322	0.5001	22.9779	36.3759
TRADES+IGR	0.6940	0.2474	0.5236	23.2356	35.0009

results also show that for a model with a larger Kendall's rank correlation, the theoretical cosine distance upper bound is more likely to be smaller (see Fig. 2), which means that the model is more difficult to be attacked. This also confirms that cosine similarity is positively correlated to Kendall's rank correlation as proposed in (Wang & Kong, 2022).

6 Conclusion

For the first time, we formulate the certified attribution robustness as a constrained optimization problem, whose optimum value is the upper bound of differences between original and perturbed attributions. The optimization problem is constrained on the size of perturbation and the unchanged classification label after being perturbed. For each of the two metrics of the attribution difference, Euclidean and cosine distances, the problem is solved to certify ℓ_2 and ℓ_∞-norm attacks based on the first-order Taylor series and the estimation of attribution gradients. Experimental results validate the certifications.

REFERENCES

Sebastian Bach, Alexander Binder, Grégoire Montavon, Frederick Klauschen, Klaus-Robert Müller, and Wojciech Samek. On pixel-wise explanations for non-linear classifier decisions by layer-wise relevance propagation. *PloS one*, 10(7):e0130140, 2015.

Umang Bhatt, Alice Xiang, Shubham Sharma, Adrian Weller, Ankur Taly, Yunhan Jia, Joydeep Ghosh, Ruchir Puri, José MF Moura, and Peter Eckersley. Explainable machine learning in deployment. In *Proceedings of the 2020 conference on fairness, accountability, and transparency*, pp. 648–657, 2020.

Akhilan Boopathy, Sijia Liu, Gaoyuan Zhang, Cynthia Liu, Pin-Yu Chen, Shiyu Chang, and Luca Daniel. Proper network interpretability helps adversarial robustness in classification. In *International Conference on Machine Learning*, pp. 1014–1023. PMLR, 2020.

Jiefeng Chen, Xi Wu, Vaibhav Rastogi, Yingyu Liang, and Somesh Jha. Robust attribution regularization. In *Advances in Neural Information Processing Systems*, pp. 14300–14310, 2019.

Jeremy Cohen, Elan Rosenfeld, and Zico Kolter. Certified adversarial robustness via randomized smoothing. In *International Conference on Machine Learning*, pp. 1310–1320. PMLR, 2019.

Ann-Kathrin Dombrowski, Maximillian Alber, Christopher Anders, Marcel Ackermann, Klaus-Robert Müller, and Pan Kessel. Explanations can be manipulated and geometry is to blame. In *Advances in Neural Information Processing Systems*, pp. 13589–13600, 2019.

Chris Finlay and Adam M Oberman. Scaleable input gradient regularization for adversarial robustness. *arXiv preprint arXiv:1905.11468*, 2019.

Amirata Ghorbani, Abubakar Abid, and James Zou. Interpretation of neural networks is fragile. In *Proceedings of the AAAI Conference on Artificial Intelligence*, volume 33, pp. 3681–3688, 2019.

Ian J Goodfellow, Jonathon Shlens, and Christian Szegedy. Explaining and harnessing adversarial examples. In *International Conference on Learning Representations*, 2015.

Bryce Goodman and Seth Flaxman. European union regulations on algorithmic decision-making and a "right to explanation". *AI magazine*, 38(3):50–57, 2017.

Hongyu Guo, Yongyi Mao, and Richong Zhang. Mixup as locally linear out-of-manifold regularization. In *Proceedings of the AAAI Conference on Artificial Intelligence*, volume 33, pp. 3714–3722, 2019.

Adam Ivankay, Ivan Girardi, Chiara Marchiori, and Pascal Frossard. Far: A general framework for attributional robustness. *arXiv preprint arXiv:2010.07393*, 2020.

José Jiménez-Luna, Francesca Grisoni, and Gisbert Schneider. Drug discovery with explainable artificial intelligence. *Nature Machine Intelligence*, 2(10):573–584, 2020.

Maurice George Kendall. Rank correlation methods. 1948.

Alex Krizhevsky. Learning multiple layers of features from tiny images. 2009.

Cassidy Laidlaw, Sahil Singla, and Soheil Feizi. Perceptual adversarial robustness: Defense against unseen threat models. In *9th International Conference on Learning Representations, ICLR 2021, Virtual Event, Austria, May 3-7, 2021*. OpenReview.net, 2021. URL https://openreview.net/forum?id=dFwBosAcJkN.

Yann LeCun, Corinna Cortes, and CJ Burges. Mnist handwritten digit database. *ATT Labs [Online]. Available: http://yann.lecun.com/exdb/mnist*, 2, 2010.

Scott M Lundberg and Su-In Lee. A unified approach to interpreting model predictions. *Advances in neural information processing systems*, 30, 2017.

Aleksander Madry, Aleksandar Makelov, Ludwig Schmidt, Dimitris Tsipras, and Adrian Vladu. Towards deep learning models resistant to adversarial attacks. In *International Conference on Learning Representations*, 2018. URL https://openreview.net/forum?id=rJzIBfZAb.

Panos M Pardalos and Stephen A Vavasis. Quadratic programming with one negative eigenvalue is np-hard. *Journal of Global optimization*, 1(1):15–22, 1991.

Chongli Qin, James Martens, Sven Gowal, Dilip Krishnan, Krishnamurthy Dvijotham, Alhussein Fawzi, Soham De, Robert Stanforth, and Pushmeet Kohli. Adversarial robustness through local linearization. *Advances in Neural Information Processing Systems*, 32, 2019.

Anindya Sarkar, Anirban Sarkar, and Vineeth N Balasubramanian. Enhanced regularizers for attributional robustness. In *Proceedings of the AAAI Conference on Artificial Intelligence*, volume 35, pp. 2532–2540, 2021.

Rory Sayres, Ankur Taly, Ehsan Rahimy, Katy Blumer, David Coz, Naama Hammel, Jonathan Krause, Arunachalam Narayanaswamy, Zahra Rastegar, Derek Wu, et al. Using a deep learning algorithm and integrated gradients explanation to assist grading for diabetic retinopathy. *Ophthalmology*, 126(4):552–564, 2019.

Avanti Shrikumar, Peyton Greenside, Anna Shcherbina, and Anshul Kundaje. Not just a black box: Learning important features through propagating activation differences. *arXiv preprint arXiv:1605.01713*, 2016.

Avanti Shrikumar, Peyton Greenside, and Anshul Kundaje. Learning important features through propagating activation differences. In *International Conference on Machine Learning*, pp. 3145–3153. PMLR, 2017.

Carl-Johann Simon-Gabriel, Yann Ollivier, Leon Bottou, Bernhard Schölkopf, and David Lopez-Paz. First-order adversarial vulnerability of neural networks and input dimension. In *International Conference on Machine Learning*, pp. 5809–5817. PMLR, 2019.

Karen Simonyan, Andrea Vedaldi, and Andrew Zisserman. Deep inside convolutional networks: Visualising image classification models and saliency maps. In *2nd International Conference on Learning Representations, ICLR 2014, Banff, AB, Canada, April 14-16, 2014, Workshop Track Proceedings*, 2014.

Amitojdeep Singh, Sourya Sengupta, and Vasudevan Lakshminarayanan. Explainable deep learning models in medical image analysis. *Journal of Imaging*, 6(6):52, 2020a.

Mayank Singh, Nupur Kumari, Puneet Mangla, Abhishek Sinha, Vineeth N Balasubramanian, and Balaji Krishnamurthy. Attributional robustness training using input-gradient spatial alignment. In *Computer Vision–ECCV 2020: 16th European Conference, Glasgow, UK, August 23–28, 2020, Proceedings, Part XXVII 16*, pp. 515–533. Springer, 2020b.

Sahil Singla and Soheil Feizi. Second-order provable defenses against adversarial attacks. In *International conference on machine learning*, pp. 8981–8991. PMLR, 2020.

Mukund Sundararajan, Ankur Taly, and Qiqi Yan. Axiomatic attribution for deep networks. In *International Conference on Machine Learning*, pp. 3319–3328. PMLR, 2017.

Fan Wang and Adams Wai-Kin Kong. Exploiting the relationship between kendall's rank correlation and cosine similarity for attribution protection. *arXiv preprint arXiv:2205.07279*, 2022.

Zifan Wang, Haofan Wang, Shakul Ramkumar, Piotr Mardziel, Matt Fredrikson, and Anupam Datta. Smoothed geometry for robust attribution. In *Advances in Neural Information Processing Systems*, volume 33, pp. 13623–13634. Curran Associates, Inc., 2020.

Han Xiao, Kashif Rasul, and Roland Vollgraf. Fashion-mnist: a novel image dataset for benchmarking machine learning algorithms. *arXiv preprint arXiv:1708.07747*, 2017.

Yao-Yuan Yang, Cyrus Rashtchian, Hongyang Zhang, Russ R Salakhutdinov, and Kamalika Chaudhuri. A closer look at accuracy vs. robustness. *Advances in neural information processing systems*, 33:8588–8601, 2020.

Matthew D Zeiler and Rob Fergus. Visualizing and understanding convolutional networks. In *European conference on computer vision*, pp. 818–833. Springer, 2014.

Hongyang Zhang, Yaodong Yu, Jiantao Jiao, Eric Xing, Laurent El Ghaoui, and Michael Jordan. Theoretically principled trade-off between robustness and accuracy. In *International Conference on Machine Learning*, pp. 7472–7482. PMLR, 2019.

Huan Zhang, Tsui-Wei Weng, Pin-Yu Chen, Cho-Jui Hsieh, and Luca Daniel. Efficient neural network robustness certification with general activation functions. *Advances in neural information processing systems*, 31, 2018.

Linjun Zhang, Zhun Deng, Kenji Kawaguchi, Amirata Ghorbani, and James Zou. How does mixup help with robustness and generalization? In *9th International Conference on Learning Representations, ICLR 2021, Virtual Event, Austria, May 3-7, 2021*. OpenReview.net, 2021. URL https://openreview.net/forum?id=8yKEo06dKNo.

Luisa M. Zintgraf, Taco S. Cohen, Tameem Adel, and Max Welling. Visualizing deep neural network decisions: Prediction difference analysis. In *International Conference on Learning Representations, ICLR 2017*. OpenReview.net, 2017. URL https://openreview.net/forum?id=BJ5UeU9xx.

A PROOFS

A.1 PROOF OF COROLLARY 1

Before we prove Corollary 1, We first introduce the following lemma.

Lemma 1. *For $0 < q < p$, the following inequality holds:*

$$\|\boldsymbol{x}\|_q \leq d^{\frac{1}{q}-\frac{1}{p}}\|\boldsymbol{x}\|_p \tag{11}$$

where $\boldsymbol{x} \in \mathbb{R}^d$.

Proof. Consider $\boldsymbol{u}, \boldsymbol{v} \in \mathbb{R}^d$, using the Hölder's Inequality that for m, n satisfying $\frac{1}{m} + \frac{1}{n} = 1$,

$$\sum_i |u_i||v_i| \leq \left(\sum_i |u_i|^m\right)^{\frac{1}{m}} \left(\sum_i |v_i|^n\right)^{\frac{1}{n}}. \tag{12}$$

If we take $|u_i| = |x_i|^q$, $v_i = 1$, $m = \frac{p}{q}$ and $n = \frac{p}{p-q}$, we get

$$\sum_i |x_i|^q \leq \left(\sum_i |x_i|^p\right)^{\frac{q}{p}} d^{\frac{p-q}{p}} \tag{13}$$

By taking the power of $\frac{1}{q}$ on both sides, we have

$$\left(\sum_i |x_i|^q\right)^{\frac{1}{q}} \leq \left(\sum_i |x_i|^p\right)^{\frac{1}{p}} d^{\frac{1}{q}-\frac{1}{p}} \tag{14}$$

which concludes the proof. □

Corollary 1. *Given a twice-differentiable classifier $f : \mathbb{R}^d \to \mathbb{R}^k$, and its attribution g^y on label y, assume that g^y is locally linear within the neighborhood of $\boldsymbol{x}$, $\mathcal{B}_\varepsilon(\boldsymbol{x}) = \{\boldsymbol{x} + \boldsymbol{\delta} | \|\boldsymbol{\delta}\|_p \leq \varepsilon\}$, then for all perturbations $\|\boldsymbol{\delta}\|_p \leq \varepsilon$ that $p > 2$, $\|g^y(\boldsymbol{x} + \boldsymbol{\delta}) - g^y(\boldsymbol{x})\|_2 \leq d^{\frac{1}{2}-\frac{1}{p}}\xi_{max}\varepsilon$, where ξ_{max} is the largest singular value of $H = \nabla g^y(\boldsymbol{x})$.*

Proof. Using Lemma 1, we have $\|\boldsymbol{\delta}\|_2 \leq d^{\frac{1}{2}-\frac{1}{p}}\|\boldsymbol{\delta}\|_p$. Similar to the proof of Theorem 1,

$$\|g^y(\boldsymbol{x} + \boldsymbol{\delta}) - g^y(\boldsymbol{x})\|_2^2 \leq \lambda_{max}\|\boldsymbol{\delta}\|_2^2 \leq \lambda_{max}\left(d^{\frac{1}{2}-\frac{1}{p}}\|\boldsymbol{\delta}\|_p\right)^2 \leq \lambda_{max}\left(d^{\frac{1}{2}-\frac{1}{p}}\varepsilon\right)^2 \tag{15}$$

Therefore,

$$\|g^y(\boldsymbol{x} + \boldsymbol{\delta}) - g^y(\boldsymbol{x})\|_2 \leq d^{\frac{1}{2}-\frac{1}{p}}\xi_{max}\varepsilon \tag{16}$$

□

A.2 PROOF OF THEOREM 2

Theorem 2. *Given a twice-differentiable classifier f, its attribution on label y, g^y, and the gradient $H = \nabla g^y$, assume that g^y is locally linear within the neighborhood of $\boldsymbol{x}$, $\mathcal{B}_\varepsilon(\boldsymbol{x}) = \{\boldsymbol{x} + \boldsymbol{\delta} | \|\boldsymbol{\delta}\|_\infty \leq \varepsilon\}$, then for all perturbations $\|\boldsymbol{\delta}\|_\infty \leq \varepsilon$,*

$$\|g^y(\boldsymbol{x} + \boldsymbol{\delta}) - g^y(\boldsymbol{x})\|_2 \leq \varepsilon\sqrt{\sum_{i,j}|P_{ij}|}. \tag{6}$$

where $P = HH^\top$ and the equality is taken at $\boldsymbol{\delta} = (\pm\varepsilon, \ldots, \pm\varepsilon)^\top$.

Proof. Recall that under the local linearity assumption,

$$\|g^y(\boldsymbol{x} + \boldsymbol{\delta}) - g^y(\boldsymbol{x})\|_2^2 \leq \boldsymbol{\delta}^\top P\boldsymbol{\delta} = \sum_{i,j} P_{ij}\delta_i\delta_j. \tag{17}$$

Since $P_{ij} \leq |P_{ij}|$ and $\delta_i\delta_j \leq \|\boldsymbol{\delta}\|_\infty^2 \leq \varepsilon^2$ for all i, j, we can easily prove the theorem that

$$\|g^y(\boldsymbol{x} + \boldsymbol{\delta}) - g^y(\boldsymbol{x})\|_2^2 \leq \varepsilon^2 \sum_{i,j}|P_{ij}|. \tag{18}$$

□

A.3 PROOF OF PROPOSITION 1

Proposition 1. *Denote the gradient-based attribution satisfying the completeness axiom of $\boldsymbol{x}$ on ground truth label y by $g^y(\boldsymbol{x})$, and the attribution on a different label y' by $g^{y'}(\boldsymbol{x})$. Given the perturbation $\boldsymbol{\delta}$, assume that g^y is locally linear within the neighborhood of $\boldsymbol{x}$, $\mathcal{B}_\varepsilon(\boldsymbol{x}) = \{\boldsymbol{x}+\boldsymbol{\delta} | \|\boldsymbol{\delta}\|_p \leq \varepsilon\}$, the classification result of $\boldsymbol{x}+\boldsymbol{\delta}$ does not change from y to y' if*

$$\left(\left(\nabla g^{y'}(\boldsymbol{x}) - \nabla g^y(\boldsymbol{x})\right)\Delta\right)^\top \boldsymbol{\delta} < f_y(\boldsymbol{x}) - f_{y'}(\boldsymbol{x}), \tag{7}$$

where Δ is an all one vector, $\Delta = (1, \ldots, 1)^\top \in \mathbb{R}^d$.

Proof. Recall that we denote the gradient-based attribution satisfying the completeness axiom of $\boldsymbol{x}$ on target label y by $g^y(\boldsymbol{x})$, *e.g.*, integrated gradients. Similarly, we denote the attribution on a different label y' by $g^{y'}(\boldsymbol{x})$. Given the perturbation $\boldsymbol{\delta}$, according to the above assumption, we can write that

$$g^y(\boldsymbol{x}+\boldsymbol{\delta}) = g^y(\boldsymbol{x}) + \nabla g^y(\boldsymbol{x})^\top \boldsymbol{\delta} \tag{19}$$

Similarly, the approximation of $g^{y'}(\boldsymbol{x}+\boldsymbol{\delta})$ is given by:

$$g^{y'}(\boldsymbol{x}+\boldsymbol{\delta}) = g^{y'}(\boldsymbol{x}) + \nabla g^{y'}(\boldsymbol{x})^\top \boldsymbol{\delta} \tag{20}$$

According to the completeness axiom, given an all one vector $\Delta = (1, \ldots, 1)^\top$, we have

$$\Delta^\top g^y(\boldsymbol{x}) = f_y(\boldsymbol{x}). \tag{21}$$

Consider the perturbation $\boldsymbol{\delta}$, if $\boldsymbol{\delta}$ does not change the label of $\boldsymbol{x}$ from y to y', then $f_{y'}(\boldsymbol{x}+\boldsymbol{\delta}) < f_y(\boldsymbol{x}+\boldsymbol{\delta})$, *i.e.*,

$$\Delta^\top g^{y'}(\boldsymbol{x}+\boldsymbol{\delta}) < \Delta^\top g^y(\boldsymbol{x}+\boldsymbol{\delta}), \tag{22}$$

which gives

$$\Delta^\top g^{y'}(\boldsymbol{x}) + \Delta^\top \nabla g^{y'}(\boldsymbol{x})^\top \boldsymbol{\delta} < \Delta^\top g^y(\boldsymbol{x}) + \Delta^\top \nabla g^y(\boldsymbol{x})^\top \boldsymbol{\delta}. \tag{23}$$

By rearranging the above inequality, we have

$$\left(\left(\nabla g^{y'}(\boldsymbol{x}) - \nabla g^y(\boldsymbol{x})\right)\Delta\right)^\top \boldsymbol{\delta} < f_y(\boldsymbol{x}) - f_{y'}(\boldsymbol{x}). \tag{24}$$

□

A.4 PROOF OF COROLLARY 2

Corollary 2. *Given a twice-differentiable classifier $f : \mathbb{R}^d \to \mathbb{R}^k$ and its attribution g^y on label y, for all perturbations $\|\boldsymbol{\delta}\|_p \leq \varepsilon$, if the Euclidean distance of $g^y(\boldsymbol{x}+\boldsymbol{\delta})$ and $g^y(\boldsymbol{x})$ is upper bounded by $T(\varepsilon; \boldsymbol{x})$, and $0 \leq T(\varepsilon; \boldsymbol{x}) \leq \|g^y(\boldsymbol{x})\|_2$, then their cosine distance (D_c) is upper bounded by*

$$D_c(g^y(\boldsymbol{x}+\boldsymbol{\delta}), g^y(\boldsymbol{x})) \leq 1 - \sqrt{1 - \frac{T(\varepsilon;\boldsymbol{x})^2}{\|g^y(\boldsymbol{x})\|_2^2}}. \tag{9}$$

Proof. The corollary can be proved using the geometric property (see Fig. 1a) that

$$\sin(g^y(\boldsymbol{x}+\boldsymbol{\delta}), g^y(\boldsymbol{x})) \leq \frac{T(\varepsilon;\boldsymbol{x})}{\|g^y(\boldsymbol{x})\|_2}, \tag{25}$$

and,

$$\begin{aligned}
\operatorname{cosd}(g^y(\boldsymbol{x}+\boldsymbol{\delta}), g^y(\boldsymbol{x})) &= 1 - \cos(g^y(\boldsymbol{x}+\boldsymbol{\delta}), g^y(\boldsymbol{x})) && (26)\\
&= 1 - \sqrt{1 - \sin^2(g^y(\boldsymbol{x}+\boldsymbol{\delta}), g^y(\boldsymbol{x}))} && (27)\\
&\leq 1 - \sqrt{1 - \frac{T(\varepsilon;\boldsymbol{x})^2}{\|g^y(\boldsymbol{x})\|_2^2}} && (28)
\end{aligned}$$

□

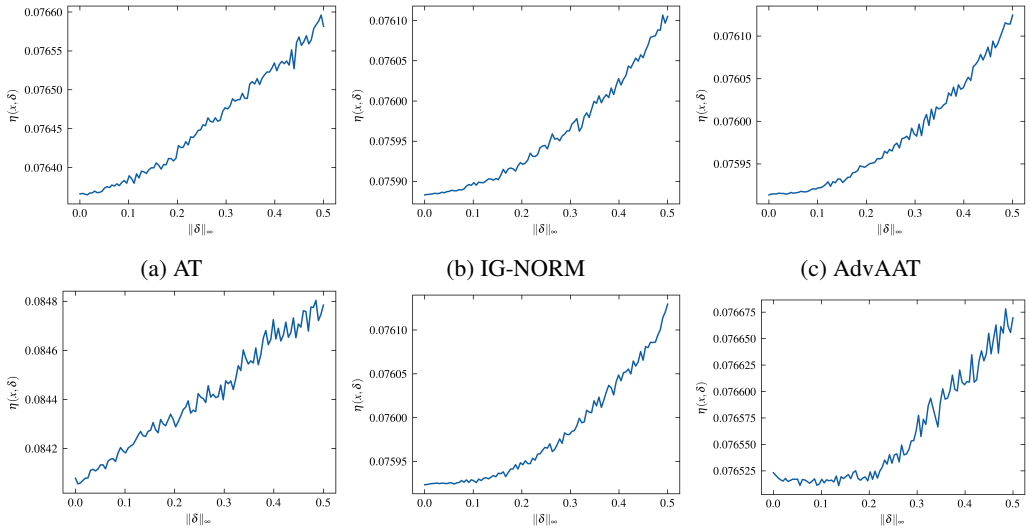

(a) AT (b) IG-NORM (c) AdvAAT

(d) ART (e) TRADES (f) TRADES+IGR

Figure 3: Values of η for different $\|\boldsymbol{\delta}\|_\infty$ computed from CIFAR-10 using integrated gradients. The magnitudes are ranging from 0.07 to 0.09 and are negligible comparing with the average norm of attributions which is 3.47 on CIFAR-10.

B Analysis of Local Linearity Assumption

B.1 Evaluation of Local Linearity Assumption of Attribution Functions

The theories of this work are based on the local linearity assumption that $g^y(\boldsymbol{x})$ is linear within $\mathcal{B}_\varepsilon(\boldsymbol{x}) = \{\boldsymbol{x} + \boldsymbol{\delta} | \|\boldsymbol{\delta}\|_p \leq \varepsilon\}$. It is worth noting that such local linearity is a valid assumption for smooth functions, which can be achieved by both adversarial and attributional robust methods. Adversarial defense methods look for locally linearity functions to reduce the impact of adversarial attacks (Qin et al., 2019; Yang et al., 2020). Similarly, attributional defense methods train for smooth gradients to defend against attribution attacks (Wang et al., 2020). It is also a common practice in related literature (Finlay & Oberman, 2019; Guo et al., 2019; Simon-Gabriel et al., 2019; Laidlaw et al., 2021; Zhang et al., 2021) to make similar assumptions.

Furthermore, the validity of this assumption also depends on the size of $\boldsymbol{\delta}$. The perturbation $\boldsymbol{\delta}$ is restricted within a small ℓ_p ball around $\boldsymbol{x}$ to ensure that the perturbed images are visually indistinguishable comparing to its original counterpart. The maximum allowable size ε for $\boldsymbol{\delta}$ is relatively small compared with the intensity range of the original image. When $\boldsymbol{\delta}$ is small, the remainder of the Taylor series of $g^y(\boldsymbol{x})$ is negligible and the local linearity assumption is valid. As shown in Figure 3, the value of $\eta(\boldsymbol{x}, \boldsymbol{\delta}) = \|g^y(\boldsymbol{x}) - g^y(\boldsymbol{x} + \boldsymbol{\delta}) - \boldsymbol{\delta}^\top \nabla g^y(\boldsymbol{x})\|_2$ is small and negligible when $\|\boldsymbol{\delta}\|_\infty$ is small.

B.2 Generalization of Theorem 1

Theorem 3. *Given a twice-differentiable classifier $f : \mathbb{R}^d \to \mathbb{R}^k$, and its attribution g^y on label y, denote the Taylor series of $g^y(\boldsymbol{x} + \boldsymbol{\delta})$ as $g^y(\boldsymbol{x}) + \boldsymbol{\delta}^\top \nabla g^y(\boldsymbol{x}) + R_1(\boldsymbol{x})$. If $-(c-1)\boldsymbol{\delta}^\top \nabla g^y(\boldsymbol{x}) \preceq R_1(\boldsymbol{x}) \preceq (c-1)\boldsymbol{\delta}^\top \nabla g^y(\boldsymbol{x})$ for a constant $c \geq 1$, where $\preceq$ refers to element-wise less than or equal to, then for all perturbations $\|\boldsymbol{\delta}\|_2 \leq \varepsilon$,*

$$\|g^y(\boldsymbol{x} + \boldsymbol{\delta}) - g^y(\boldsymbol{x})\|_2 \leq c\xi_{max}\varepsilon,$$

where ξ_{max} is the largest singular value of $H = \nabla g^y(\boldsymbol{x})$.

Proof. Based on the Taylor series of $g^y(\boldsymbol{x})$ and the above condition, we have

$$\|g^y(\boldsymbol{x}+\boldsymbol{\delta}) - g^y(\boldsymbol{x})\|_2^2 \leq \|\boldsymbol{\delta}^\top \nabla g^y(\boldsymbol{x}) + (c-1)\boldsymbol{\delta}^\top \nabla g^y(\boldsymbol{x})\|_2^2 = c^2 \boldsymbol{\delta}^\top \nabla g^y(\boldsymbol{x}) \nabla g^y(\boldsymbol{x})^\top \boldsymbol{\delta} \quad (29)$$

$$= c^2 \frac{\boldsymbol{\delta}^\top}{\|\boldsymbol{\delta}\|_2} P \frac{\boldsymbol{\delta}}{\|\boldsymbol{\delta}\|_2} \cdot \|\boldsymbol{\delta}\|_2^2 \quad (30)$$

$$\leq c^2 \lambda_{max} \|\boldsymbol{\delta}\|_2^2 \leq c^2 \lambda_{max} \varepsilon^2 \quad (31)$$

where λ_{max} is the largest eigenvalue of $P = HH^\top = \nabla g^y(\boldsymbol{x}) \nabla g^y(\boldsymbol{x})^\top$, and $\boldsymbol{v}_{max}$ is the corresponding eigenvector. The equality in Eq. 31 is achieved when $\boldsymbol{\delta}$ is $\varepsilon \boldsymbol{v}_{max}$ or $-\varepsilon \boldsymbol{v}_{max}$. Since the singular values of H are equal to the square root of the eigenvalues of P, then,

$$\|g^y(\boldsymbol{x}+\boldsymbol{\delta}) - g^y(\boldsymbol{x})\|_2 \leq c\sqrt{\lambda_{max}}\varepsilon = c\xi_{max}\varepsilon. \quad (32)$$

□

This is a generalized version of Theorem 1 that is applicable for all twice-differentiable classifiers. Under local linearity assumption, $R_1(\boldsymbol{x}) = 0$, which means $c = 1$, the result coincides with the original version of Theorem 1.

B.3 Derivation of Eq. (10)

By Taylor expansion, $g^y(\boldsymbol{x}+\boldsymbol{\delta}) - g^y(\boldsymbol{x}) = \boldsymbol{\delta}^\top \nabla g^y(\boldsymbol{x}) + R_1(\boldsymbol{x})$, where R_1 is the first order Taylor remainder. Thus, we have

$$\|R_1(\boldsymbol{x})\|_2 \geq \|g^y(\boldsymbol{x}+\boldsymbol{\delta}) - g^y(\boldsymbol{x})\|_2 - \|\boldsymbol{\delta}^\top \nabla g^y(\boldsymbol{x})\|_2 \quad (33)$$

Take $c = \frac{\|R_1(\boldsymbol{x})\|_2}{\|\boldsymbol{\delta}^\top \nabla g^y(\boldsymbol{x})\|_2} + 1$,

$$\|\boldsymbol{\delta}^\top \nabla g^y(\boldsymbol{x})\|_2 + \|R_1(\boldsymbol{x})\|_2 = c\|\boldsymbol{\delta}^\top \nabla g^y(\boldsymbol{x})\|_2, \quad (34)$$

and it would be the worst-case for the linear assumption when $\boldsymbol{\delta} = \varepsilon \boldsymbol{v}_{max}$. By taking $\varepsilon \boldsymbol{v}_{max}$ as $\boldsymbol{\delta}$, $\|R_1(\boldsymbol{x})\|_2$ can be estimated by

$$\max\left\{0, \|g^y(\boldsymbol{x}+\varepsilon \boldsymbol{v}_{max}) - g^y(\boldsymbol{x})\|_2 - \|\varepsilon \boldsymbol{v}_{max}^\top \nabla g^y(\boldsymbol{x})\|_2\right\}. \quad (35)$$

Since $\|g^y(\boldsymbol{x}+\varepsilon \boldsymbol{v}_{max}) - g^y(\boldsymbol{x})\|_2 - \|\varepsilon \boldsymbol{v}_{max}^\top \nabla g^y(\boldsymbol{x})\|_2 \leq \|R_1(\boldsymbol{x})\|_2$. Putting Eq. (35) into c and using the result in Eq. (5), we have

$$c = \max\left\{0, \frac{\|g^y(\boldsymbol{x}+\varepsilon \boldsymbol{v}_{max}) - g^y(\boldsymbol{x})\|_2 - \|\varepsilon \boldsymbol{v}_{max}^\top \nabla g^y(\boldsymbol{x})\|_2}{\xi_{max}\varepsilon}\right\} + 1 \quad (36)$$

$$= \max\left\{1, \frac{\|g^y(\boldsymbol{x}+\varepsilon \boldsymbol{v}_{max}) - g^y(\boldsymbol{x})\|_2}{\xi_{max}\varepsilon}\right\}. \quad (37)$$

C Analysis of Attribution Gradients

C.1 The Gradient of Integrated Gradients

We provide the justification showing that the gradient of IG is diagonal-dominated. Consider that

$$\text{IG}(\boldsymbol{x})_i = x_i \times \frac{1}{m} \sum_{\alpha=1}^{m} \frac{\partial f(\frac{\alpha}{m}\boldsymbol{x})}{\partial x_i} \quad (38)$$

and

$$\nabla \text{IG}(\boldsymbol{x})_{ij} = \frac{\partial \text{IG}(\boldsymbol{x})_i}{\partial x_j} \quad (39)$$

If $i \neq j$, then

$$\frac{\partial \text{IG}(\boldsymbol{x})_i}{\partial x_j} = x_i \cdot \frac{1}{m} \sum_{\alpha=1}^{m} \frac{\partial^2 f(\frac{\alpha}{m}\boldsymbol{x})}{\partial x_i \partial x_j} \times \frac{\alpha}{m} \quad (40)$$

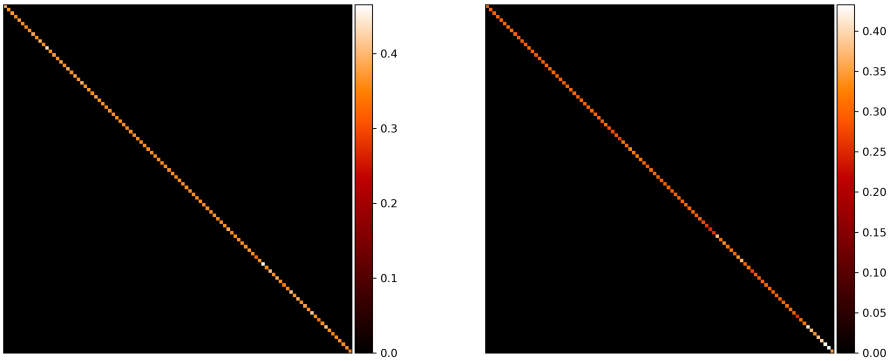

(a) (b)

Figure 4: The first 100 dimensions of gradient attribution generated from (a) MNIST and (b) Fashion-MNIST.

If $i = j$, then

$$\frac{\partial \text{IG}(\boldsymbol{x})_i}{\partial x_j} = \frac{1}{m}\sum_{\alpha=1}^{m}\frac{\partial f(\frac{\alpha}{m}\boldsymbol{x})}{\partial x_j} + x_i \cdot \frac{1}{m}\sum_{\alpha=1}^{m}\frac{\partial^2 f(\frac{\alpha}{m}\boldsymbol{x})}{\partial x_i \partial x_j} \times \frac{\alpha}{m} \tag{41}$$

Denote that $H_{ij}^{(\alpha)} = \frac{\partial^2 f(\frac{\alpha}{m}\boldsymbol{x})}{\partial x_i \partial x_j}$, *i.e.*, $H^{(\alpha)}$ is the Hessian matrix of $f(\frac{\alpha}{m}\boldsymbol{x})$. Thus

$$\frac{\partial \text{IG}(\boldsymbol{x})_i}{\partial x_j} = \begin{cases} \frac{1}{m}\sum_{\alpha=1}^{m}\nabla f(\frac{\alpha}{m}\boldsymbol{x}) + x_i \cdot \frac{\alpha}{m^2}H_{ij}^{(\alpha)}, & i = j \\ x_i \cdot \sum_{\alpha=1}^{m}\frac{\alpha}{m^2}H_{ij}^{(\alpha)}, & i \neq j \end{cases} \tag{42}$$

In matrix form,

$$\nabla \text{IG} = \text{diag}\left(\frac{1}{m}\sum_{\alpha=1}^{m}\nabla f(\frac{\alpha}{m}\boldsymbol{x})\right) + [\boldsymbol{x}, \cdots, \boldsymbol{x}] \otimes \frac{\alpha}{m^2}\sum_{\alpha=1}^{m}H^{(\alpha)} \tag{43}$$

If we use softplus as an activation function, *i.e.*, $g(\boldsymbol{x}) = \frac{1}{\beta}\log(1 + \exp(\beta\boldsymbol{x}))$, then,

$$g''(\boldsymbol{x}) = \frac{\beta e^{\beta\boldsymbol{x}}}{(e^{\beta\boldsymbol{x}} + 1)^2} \tag{44}$$

and

$$\lim_{\beta\to\infty} g''(\boldsymbol{x}) = 0 \tag{45}$$

As $\beta \to \infty$, $H^{(\alpha)}$ will tend to 0, and the second term in Eq. 43 will tend to 0. At the same time, if we choose the number of steps in IG, m larger, $\frac{\alpha}{m^2}$ will converge to 0 faster than $\frac{1}{m}$. Therefore, ∇IG will be diagonal-dominated.

C.2 Additional Visualization of Attribution Gradients

We provide the first 100-dimensions heatmaps of absolute values of attribution gradients, *i.e.*, gradients of IG, on MNIST and Fashion-MNIST in addition to CIFAR-10 presented in Fig. 1b. Moreover, the complete heatmaps for all the three datasets are also presented. As observed in Figs. 4 to 7, the matrices of attribution gradients are diagonal-dominant.

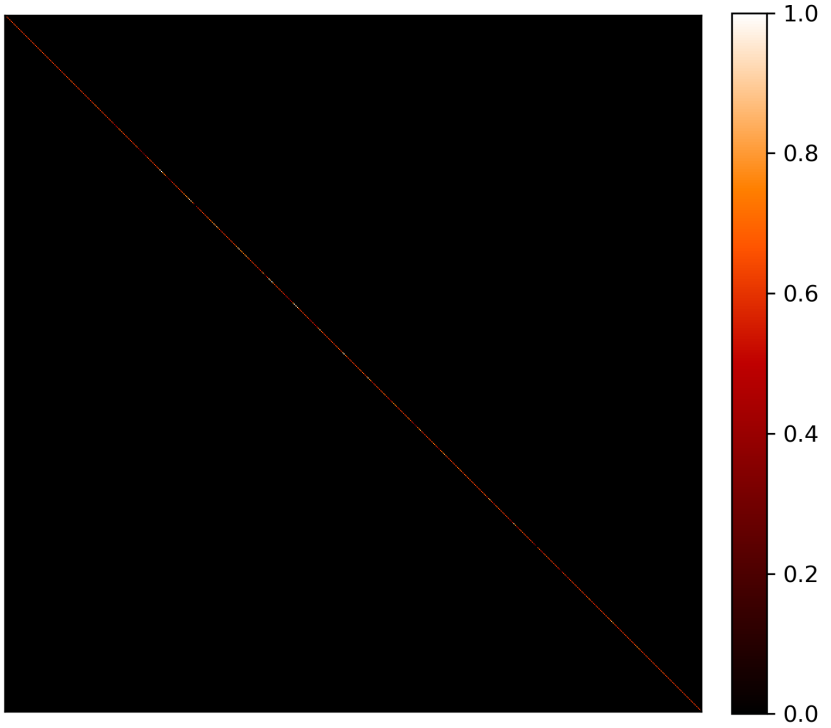

Figure 5: The full heatmap of attribution gradients of MNIST in size 784×784.

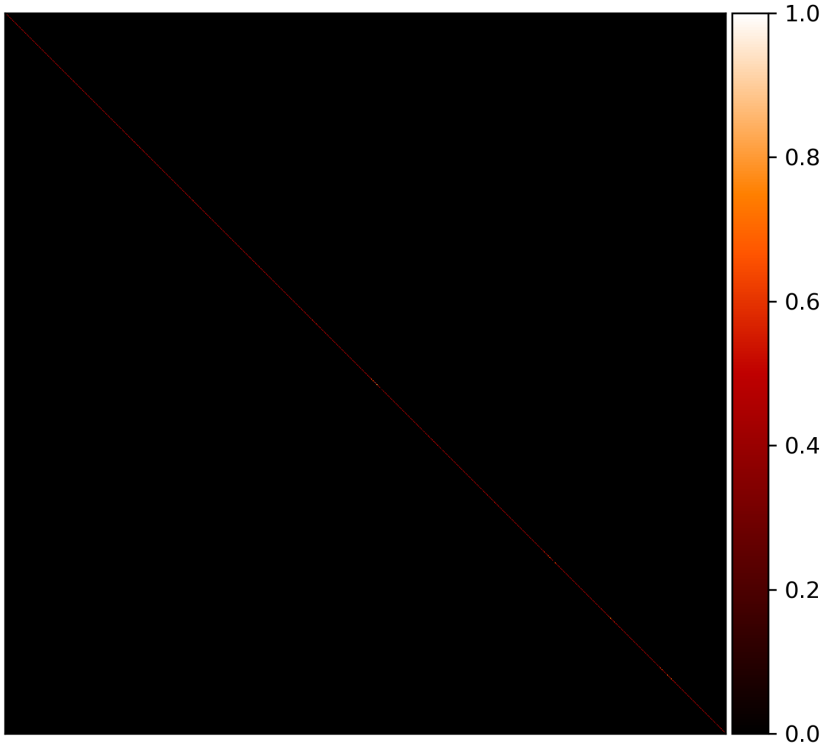

Figure 6: The full heatmap of attribution gradients of Fashion-MNIST in size 784×784.

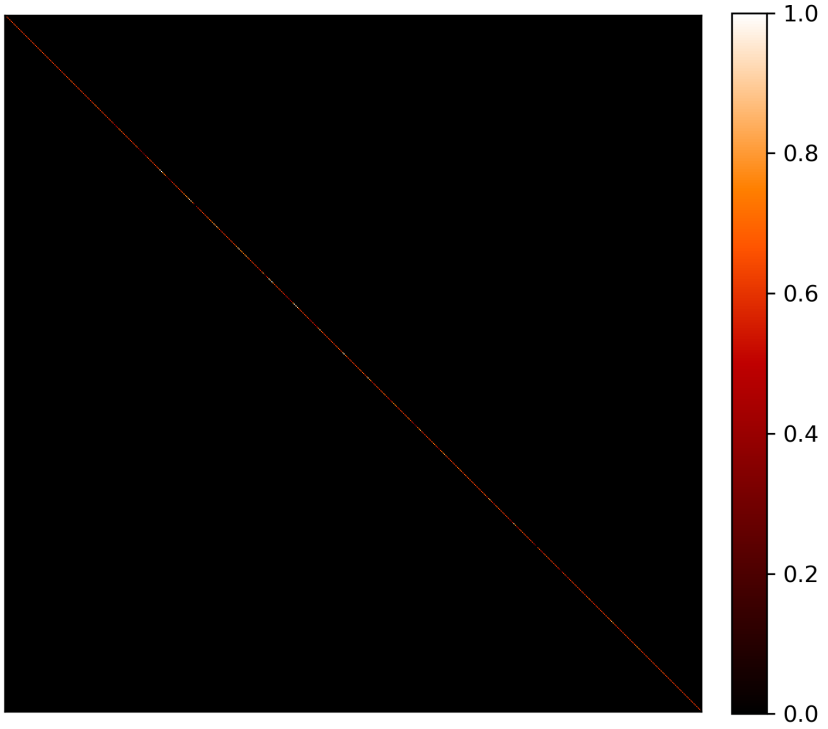

Figure 7: The full heatmap of attribution gradients of CIFAR-100 in size 3072×3072.

Table 5: Evaluation of certification without the label constraint. The cosine distance values $\widehat{T}_c$ and $\widehat{T}'_c$ are converted to degrees for easier comparison.

	SM					Input*gradient					IG				
ℓ_2	$\widehat{T}_e$	T_e	T'_e	$\widehat{T}_c$	T_c	$\widehat{T}_e$	T_e	T'_e	$\widehat{T}_c$	T_c	$\widehat{T}_e$	T_e	T'_e	$\widehat{T}_c$	T_c
AT	0.44	0.94	0.98	9.19	14.87	0.07	0.63	0.63	1.17	4.34	0.04	0.25	0.25	2.73	4.77
IG-NORM	0.03	0.70	0.79	4.33	9.06	0.03	0.50	0.52	1.40	4.75	0.01	0.16	0.16	1.65	4.37
AdvAAT	0.30	1.83	1.83	11.24	20.44	0.08	0.66	0.67	1.84	3.79	0.04	0.24	0.24	0.28	3.82
ART	0.18	0.79	0.81	10.88	14.21	0.09	0.92	0.97	0.83	6.06	0.07	0.23	0.23	0.59	4.21
TRADES	0.11	0.76	0.76	10.01	18.40	0.05	0.48	0.48	1.19	3.20	0.03	0.17	0.17	1.91	3.87
ℓ_∞															
AT	0.55	1.27	-	23.47	30.18	0.63	0.73	-	9.28	61.03	0.41	0.76	-	26.62	45.32
IG-NORM	0.42	0.70	-	25.16	32.60	0.21	0.70	-	6.88	42.94	0.20	0.48	-	21.63	35.30
AdvAAT	0.64	1.83	-	25.20	31.25	0.07	0.74	-	7.79	45.16	0.23	0.52	-	28.73	39.40
ART	0.49	1.01	-	23.81	35.17	0.27	0.79	-	10.21	48.30	0.31	0.67	-	31.01	35.64
TRADES	0.39	0.75	-	22.40	29.10	0.33	0.69	-	9.17	52.63	0.23	0.50	-	22.98	36.38

D Additional Experimental Results

D.1 Additional Results on More Models of Certification without the Label Constraint

In this subsection, we evaluate the certification without the label constraint for the other models, apart from TRADES+IGR in the paper. The perturbation size is chosen to be 0.1 for all evaluations. As in Sec. 5, we use Theorem 1 and 2 to compute $T_e = \xi_{max}\varepsilon$ and extend it to T_c using Eq. 9. The modified upper bound $T'_e = c\xi_{max}\varepsilon$ is also provided to address the inaccurate Taylor approximation (less than 1%). $\widehat{T}_e$ and $\widehat{T}_c$ are computed from the corresponding average attribution differences. The results are given in Table 5. It is shown that the sample distances under both Euclidean and cosine metrics are bounded by T'_e and T_c as expected. All the distortion caused by the attacks *i.e.*, $\widehat{T}_e$ and $\widehat{T}_c$ are smaller than T'_e and T_c.

Table 6: Evaluation of ℓ_2-norm certification with the label constraint on MNIST, Fashion-MNIST and CIFAR-10 using different ε.

	$\widehat{T}_e$	T_e	T'_e	$\widehat{T}_c$(deg)	T_c(deg)	$\widehat{T}_e$	T_e	T'_e	$\widehat{T}_c$(deg)	T_c(deg)
MNIST			$\varepsilon = 0.1$					$\varepsilon = 0.2$		
AT	0.0856	0.3074	0.3101	4.6026	14.3020	0.1176	0.4611	0.4617	5.9845	29.6082
IG-NORM	0.1436	0.5776	0.5776	3.9514	14.6430	0.2094	0.8664	0.8679	5.4824	30.3707
AdvAAT	0.0938	0.7182	0.7193	2.1315	13.8325	0.1346	1.0773	1.1013	2.8725	28.5660
ART	0.2031	0.6538	0.6542	6.4244	13.9011	0.2302	0.9807	0.9993	8.5982	28.7175
TRADES	0.2159	1.0120	1.0812	3.4791	14.1049	0.3281	1.5180	1.5211	4.9429	29.1695
TRADES+IGR	0.2171	0.9928	1.0101	3.4171	14.0621	0.3032	1.4892	1.4892	4.5166	29.0745
Fashion-MNIST			$\varepsilon = 0.1$					$\varepsilon = 0.2$		
AT	0.1080	0.1400	0.1401	16.7770	26.6451	0.1413	0.2100	0.2119	21.3901	63.7570
IG-NORM	0.1232	0.3578	0.3578	8.9312	17.8256	0.1771	0.5367	0.5371	12.5177	37.7516
AdvAAT	0.1500	0.3470	0.3533	7.3499	19.0014	0.1984	0.5205	0.5209	9.4643	40.6308
ART	0.2057	0.2774	0.2775	11.6920	19.9515	0.2343	0.4161	0.4161	13.4216	43.0352
TRADES	0.0797	0.1926	0.1987	10.5544	24.7845	0.1050	0.2889	0.2889	13.8358	56.9729
TRADES+IGR	0.0672	0.0906	0.0906	11.3338	17.9020	0.0879	0.1359	0.1510	14.7998	37.9358
CIFAR-10			$\varepsilon = 0.2$					$\varepsilon = 0.3$		
AT	0.0607	0.5064	0.5064	3.7975	9.5783	0.0858	1.2661	1.2661	5.2981	24.5816
IG-NORM	0.0123	0.3164	0.3164	1.4311	8.7679	0.0592	0.7910	0.7910	6.9460	22.4006
AdvAAT	0.0300	0.4772	0.4775	1.7094	7.6575	0.0548	1.1933	1.1933	3.0553	19.4588
ART	0.0501	0.4556	0.4699	3.1004	8.4476	0.0718	1.1391	1.1420	6.3493	21.5468
TRADES	0.0360	0.3468	0.3468	3.9435	7.7550	0.0528	0.8671	0.8780	5.7514	19.7151
TRADES+IGR	0.0395	0.3384	0.3385	4.1222	7.6942	0.0577	0.8460	0.8460	5.9201	19.5551

D.2 Ablation Study of Certification Using Different ε

In this subsection, we provide more experimental results of certifications on MNIST, Fashion-MNIST and CIFAR-10 in both ℓ_2 and ℓ_∞ cases under label constraint. More specifically, for MNIST and Fashion-MNIST, we additionally provide results of $\varepsilon = 0.1$ and $\varepsilon = 0.2$ in ℓ_2 case, and $\varepsilon = 0.01$ and $\varepsilon = 0.03$ in ℓ_∞ case. For CIFAR-10, we provide $\varepsilon = 0.2$ and $\varepsilon = 0.3$ for ℓ_2 case, and $\varepsilon = 4/255$ and $\varepsilon = 8/255$ in ℓ_∞ case. The results are presented in Tables 6 and 7. For ℓ_2 constrained certification, we also provide the modified upper bound T'_e as in Sec. 5 since the Taylor approximations are inaccurate occasionally ($0 \sim 6\%$). For all tested ε, it is noticed that the theoretical bounds bound the sample Euclidean and cosine distance above. In some cases, the means of T_e and T'_e are the same because T_e bound $\widehat{T}_e$ well and the c in Eq. (10) equals to 1 for T'_e. As in Sec. 5, for ℓ_∞ case, we do not present the results of T'_e, because T_e has bounded all $\widehat{T}_e$ above.

D.3 Evaluation of the Tightness of Bounds

In addition, we further report the minimum Euclidean gaps between samples and bounds in Table 8 to measure the tightness of the provided bounds, which is defined as

$$r = \min_{0 \le i \le n} T_e^{(i)} - \widehat{T}_e^{(i)} \tag{46}$$

Note that the superscript (i) represents the i-th sample and $T_e^{(i)}$ is replaced by $T_e'^{(i)}$ in ℓ_2-norm cases. r is a straightforward measurement of the theoretical bound. We notice that although the mean of theoretical bounds sometimes are multiple times larger than the sample mean distance, the tightest bound can be only 10^{-4} greater than the sample distance. We also observe that the values of r are all positive, which also indicates that there is no perturbed attribution that violates our theoretical bound.

In addition, in Fig. 8, we also provide the visualizations of the distribution of the gap between theoretical bounds and attribution differences from real data. The values are directly computed using $T_e^{(i)} - \widehat{T}_e^{(i)}$. As we can observe from the figures, all values are positive, which verifies the validity of our bounds, and most of the values are lying close to 0, which shows the tightness of the bounds.

Table 7: Evaluation of ℓ_∞-norm certification with the label constraint on MNIST, Fashion-MNIST and CIFAR-10 with different ε.

	$\widehat{T}_e$	T_e	$\widehat{T}_c$(deg)	T_c(deg)	$\widehat{T}_e$	T_e	$\widehat{T}_c$(deg)	T_c(deg)
MNIST	$\varepsilon = 0.01$				$\varepsilon = 0.03$			
AT	0.0556	0.1550	2.9408	7.1839	0.0888	0.4651	4.2516	22.0345
IG-NORM	0.1005	0.2409	2.8745	6.0632	0.1710	0.7228	4.4179	18.4742
AdvAAT	0.0608	0.4398	1.4264	5.0839	0.1280	1.3195	2.4883	15.4170
ART	0.0767	0.5644	2.8025	10.3833	0.3617	1.6931	9.3505	32.7312
TRADES	0.1634	0.4443	2.7539	6.3323	0.3193	1.3330	4.7523	19.3224
TRADES+IGR	0.1744	0.4077	2.7731	5.1333	0.2932	1.2232	4.2425	15.5702
Fashion-MNIST	$\varepsilon = 0.01$				$\varepsilon = 0.03$			
AT	0.0516	0.0560	6.5146	9.4467	0.1043	0.1680	16.4165	29.4979
IG-NORM	0.0611	0.1113	4.7737	8.3315	0.1137	0.3339	8.1315	25.7661
AdvAAT	0.0987	0.1841	5.3706	8.1184	0.1616	0.5523	7.9204	25.0658
ART	0.0660	0.1443	6.6582	9.2791	0.3946	0.4329	23.0589	28.9294
TRADES	0.0509	0.0907	7.0612	9.0233	0.0804	0.2721	10.8579	28.0672
TRADES+IGR	0.0363	0.0505	7.1214	8.0541	0.0716	0.1515	12.1090	24.8550
CIFAR-10	$\varepsilon = 4/255$				$\varepsilon = 8/255$			
AT	0.0894	0.1200	6.0843	6.4041	0.1549	0.2400	10.5129	12.8901
IG-NORM	0.0388	0.0750	4.5743	5.2004	0.0700	0.1501	8.1882	10.4443
AdvAAT	0.0776	0.0817	2.2657	5.7139	0.0959	0.1635	3.8595	11.4857
ART	0.0722	0.1056	4.3010	5.2445	0.1281	0.2113	8.4555	10.5337
TRADES	0.0539	0.0784	3.6093	5.3381	0.0909	0.1569	9.3571	10.7232
TRADES+IGR	0.0589	0.0821	3.8230	5.1622	0.0978	0.1643	9.5879	10.3668

Table 8: Evaluation of tightness of the bounds in Euclidean distance for ℓ_2 and ℓ_∞ cases.

	MNIST			Fashion-MNIST			CIFAR-10		
$\ell_2(\varepsilon =)$	0.05	0.1	0.2	0.05	0.1	0.2	0.1	0.2	0.3
AT	0.0260	0.0320	0.0140	0.0078	0.0130	0.1207	0.0004	0.0045	0.0134
IG-NORM	0.0391	0.0597	0.0291	0.0121	0.0171	0.0742	0.0016	0.0210	0.0448
AdvAAT	0.0290	0.0465	0.0294	0.0103	0.0167	0.0183	0.0037	0.0090	0.0181
ART	0.0178	0.0115	0.0182	0.0029	0.0239	0.0011	0.0019	0.0031	0.0141
TRADES	0.0014	0.0032	0.0104	0.0037	0.0082	0.0723	0.0028	0.0048	0.0147
TRADES+IGR	0.0010	0.0038	0.0041	0.0064	0.0134	0.0385	0.0016	0.0100	0.0126
$\ell_\infty(\varepsilon =)$	0.01	0.03	0.05	0.01	0.03	0.05	4/255	8/255	0.1
AT	0.0021	0.0035	0.0117	0.0004	0.0352	0.0708	0.0025	0.0053	0.1381
IG-NORM	0.0001	0.0062	0.0105	0.0010	0.0590	0.1069	0.0026	0.0145	0.0003
AdvAAT	0.0004	0.0223	0.0901	0.0136	0.0847	0.1665	0.0448	0.1513	0.2078
ART	0.0082	0.0112	0.0233	0.0424	0.1049	0.1467	0.0118	0.0412	0.0870
TRADES	0.0001	0.0046	0.0026	0.0014	0.0337	0.0634	0.0068	0.0043	0.0530
TRADES+IGR	0.0016	0.0143	0.1389	0.0014	0.0375	0.0682	0.0016	0.0090	0.0197

Table 9: Evaluation of certification with the label constraint on Flower dataset. The numbers in the brackets indicate the percentages that attacked attribution is outside the T_e.

	ℓ_2					ℓ_∞			
	$\widehat{T}_e$	T_e	T'_e	$\widehat{T}_c$(deg)	T_c(deg)	$\widehat{T}_e$	T_e	$\widehat{T}_c$(deg)	T_c(deg)
AT	0.0170	0.0341 [2.17%]	0.0447	1.3165	1.9806	0.0238	0.4100	2.1937	13.4811
AdvAAT	0.0295	0.1424 [0.00%]	0.1424	1.5568	2.2835	0.0472	0.1025	1.4130	11.8732
TRADES	0.0220	0.0534 [0.72%]	0.0592	1.3383	3.1567	0.0182	0.1081	3.3887	11.9829
TRADES+IGR	0.0080	0.0219 [0.72%]	0.0262	0.8870	2.1255	0.0242	0.2873	1.5930	12.5584

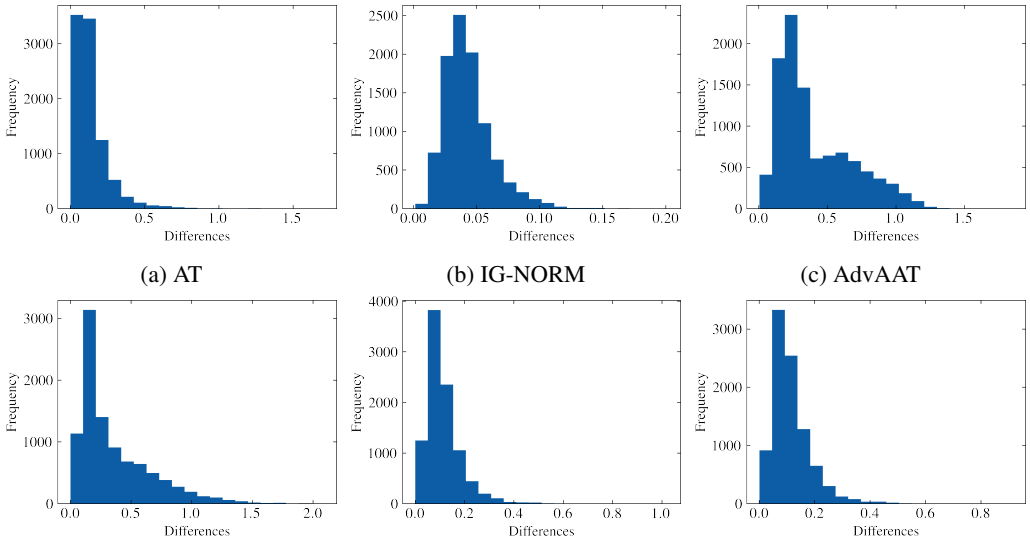

(a) AT (b) IG-NORM (c) AdvAAT

(d) ART (e) TRADES (f) TRADES+IGR

Figure 8: Distributions of differences between computed bounds and attribution differences from CIFAR-10.

D.4 Certification of ℓ_2 and ℓ_∞ Certification on Larger Size Images.

In this subsection, we evaluate our certification methods based on label constraints on Flower [2], which contains images of size $128 \times 128 \times 3$. We choose $\varepsilon = 0.1$ for both ℓ_2 and ℓ_∞ cases to compute T_e and T_c, as well as the modified bound T_e', as introduced in Sec. 5. The sample distance $\widehat{T}_e$ and $\widehat{T}_c$ are computed from the mean of distances between perturbed and original attributions, where PGD-20 is used as ℓ_2 attack and IFIA is used as ℓ_∞ attack. The results are presented in Table 9.

We notice that the theoretical bounds are valid for larger size images, where all angular and modified Euclidean bound are effectively certifying the maximum discrepancy of perturbed attributions. It worths noting that the computation load of the proposed methods for ℓ_2-norm constrained certification becomes heavier for high-dimensional cases due to the computation of eigenvalues for large matrices. For ℓ_∞ case, these eigenvalue computations have been avoided. We will study the scalability of our methods in future work.

E Alternative Formulation of Certified Robustness

The formulation of Eq. 1 can be rewritten in an equivalent form to find the maximum ε subject to the attribution difference under certain threshold ω. Formally, the formulation can be written as

$$\begin{aligned} \max \quad & \varepsilon \\ \text{s.t.} \quad & D(g^y(\boldsymbol{x}), g^y(\boldsymbol{x}+\boldsymbol{\delta})) \leq \omega \\ & \|\boldsymbol{\delta}\|_p \leq \varepsilon \\ & \arg\max_k f_k(\boldsymbol{x}) = \arg\max_k f_k(\boldsymbol{x}+\boldsymbol{\delta}) \end{aligned} \tag{47}$$

Under the above formulation, we can use the theoretical bound derived using Eq. 1 to find the corresponding optimal ε. For the ℓ_2-norm certification with or without the label constraint, when $D(\cdot,\cdot)$ is the ℓ_2 distance, the maximum ε can be computed using the upper bound $\xi_{max}\varepsilon$ derived in

[2] https://www.robots.ox.ac.uk/~vgg/data/flowers/17/index.html

Theorem 1,

$$\max_{\boldsymbol{\delta}} \|g^y(\boldsymbol{x}+\boldsymbol{\delta}) - g^y(\boldsymbol{x})\|_2 = \xi_{max}\varepsilon \leq \omega \tag{48}$$

$$\Rightarrow \varepsilon \leq \frac{\omega}{\xi_{max}} \tag{49}$$

Similarly, the maximum ε when $D(\cdot,\cdot)$ is cosine distance can be derived using Corollary 2 as

$$\max_{\boldsymbol{\delta}} D_c(g^y(\boldsymbol{x}+\boldsymbol{\delta}), g^y(\boldsymbol{x})) = 1 - \sqrt{1 - \frac{\xi_{max}\varepsilon}{\|g^y(\boldsymbol{x})\|_2^2}} \leq \omega \tag{50}$$

$$\Rightarrow \varepsilon \leq \frac{\|g(\boldsymbol{x})\|_2^2}{\xi_{max}} \left(1 - (1-\omega)^2\right) \tag{51}$$

The maximum ε for the ℓ_∞ constraint case with and without the label constraint can be also derived in the same way using the relaxed upper bound in Theorem 2. Since the Kendall's rank correlation is discontinuous, researchers proposed to use cosine similarity and ℓ_p distance to measure the similarity/dissimilarity between attributions from attacked samples and original samples (Wang & Kong, 2022; Chen et al., 2019; Boopathy et al., 2020). Thus, in this work, we derive the bounds for cosine similarity and Euclidean distance.